

Evaluation of Nasal Airflow and Resistance: Computational Modeling for Experimental Measurements

Shoji KANEDA^{*1}, Masahiro IIDA^{*1}, Hikaru YAMAMOTO^{*1}, Motoki SEKINE^{*1}, Koji EBISUMOTO^{*1}, Akihiro SAKAI^{*1} and Yoko TAKAKURA^{*2}

^{*1}Department of Otolaryngology, Tokai University School of Medicine

^{*2}Course of Science and Technology, Tokai University

(Received May 17, 2019; Accepted June 26, 2019)

Objective: When evaluating nasal obstruction, conventional measurements of nasal patency do not necessarily correspond to a patient's subjective symptoms. The aim of this research is to seek an objective evaluation method by establishing computational modeling for nasal patency measurements.

Methods: We created a computer-generated geometrical model of the nasal cavity from computed-tomography scans of an adult male, presented a computational modeling method for evaluating the nasal patency in the deep-breathing state, and simulated numerically the airflow within the nasal cavity in the natural- and deep-breathing states.

Results: During inhalation in the natural-breathing state, the airflow was higher in the center of the nasal cavity and lower in the upper and lower portions, with the airflow characteristics being associated with the nasal functions. In the deep-breathing state, the computed nasal patency was compared with that measured experimentally by rhinomanometry. The quantitative accordance between computation and experiment was unsatisfactory, but the qualitative tendencies were similar.

Conclusion: Through natural- and deep-breathing computations, the roles and functions of the olfactory region, nasal valve, and middle and inferior meatuses were evaluated from the flow patterns and pressure, with correlation to the nasal resistance and physiology. Above all, from the deep-breathing computation using the present computational modeling, it was deduced that the pressure difference is essential for determining the nasal sites at which the nasal resistance was produced. Thus, numerical simulation with computational modeling is potentially an objective method for evaluating nasal obstruction.

Key words: nasal airflow, nasal resistance, computational fluid dynamics, rhinomanometry

INTRODUCTION

Currently, rhinomanometry and acoustic rhinometry are used to measure nasal patency in the evaluation of nasal obstruction, [1]. However, in the authors' experience, nasal patency does not necessarily correspond to a patient's subjective symptoms of nasal obstruction. Recently, experimental and computational methods for evaluating nasal airflow have been reported despite the anatomical complexity involved.

Although in vivo experiments preserve the natural nasal condition (e.g., the properties of the mucosal swelling and the form of the nose) and are thus the most realistic type of experiment, direct measurements in the human nasal cavity are very difficult because of the complicated geometry therein. Computational fluid dynamics (CFD) is now a popular means of modeling airways because it avoids many of the difficulties inherent in physical experiments, [2] and its predictions agree well with particle image velocimetry measurements, [3, 4]. For example, Wakayama *et al.* used CFD to investigate how nasal obstruction affected continuous positive airway pressure treatment [5] to interpret

the flows within the human nasal cavity; simplified models [6, 7] are designed and the flow patterns are compared with those of an anatomically realistic model [8].

The aviation, automotive, railroad, and marine industries, among others, conduct aerodynamic evaluations by simulating flows numerically. Therefore, using numerical flow simulation to quantify nasal-cavity airflow is considered to be an objective method for evaluating nasal cavity airflow. This will give us a better understanding of the site-specific anatomical significance of the nasal cavity, allowing us to identify the relationship between a patient's subjective symptoms and nasal-cavity airflow and thus perform the necessary surgical procedures.

We have previously investigated the airflow patterns within nasal-cavity models by using in vitro experiments [9] and numerical simulations [10]. Based on the agreement between the results of those two approaches, we deduced the roles and functions of the nasal structural elements by comparing the airflows in an anatomically realistic model and various simplified models [10]. We have also investigated how various

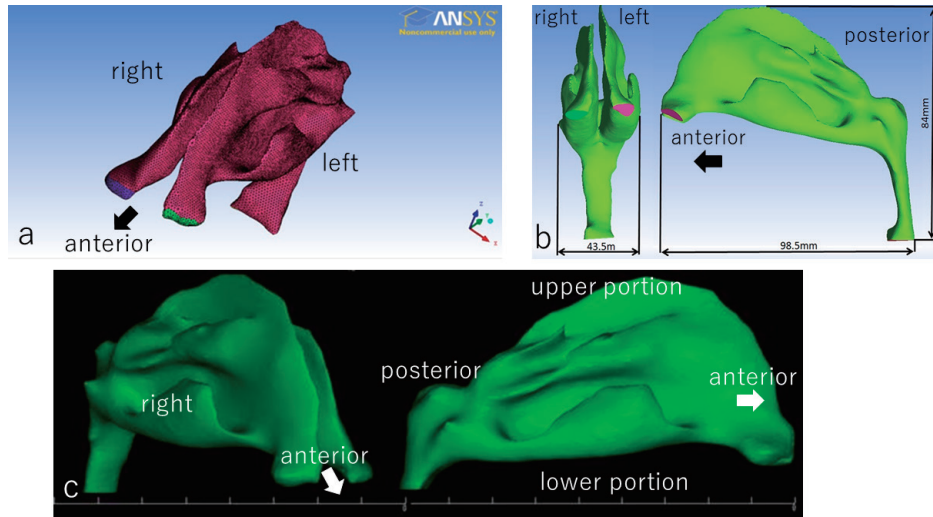


Fig. 1 Nasal model

This is the nasal model generated from CT scans of a 32-year-old male who had undergone septoplasty. We performed numerical simulation using this model.

simplified sinus-ostium models affect the airflow patterns within an anatomically realistic nasal-cavity model with a maxillary sinus (the largest of the four paranasal sinuses), and we have discussed the function of the sinus ostia in sinus ventilation [11, 12]. Those previous studies helped us recognize the site-specific anatomical significance and its physiology. Meanwhile, we have also investigated the use of numerical simulation for evaluating nasal resistance as a means of diagnosis and for guiding the surgical procedures needed to alleviate nasal obstruction [13, 14]. Our previous results suggested that numerical simulation could be (i) a way to relate nasal-cavity patency even more to the roles and functions of the nasal structural elements and (ii) a pre/post-operative means of assessing the nasal cavity and paranasal sinuses.

Herein, we present the results of numerical simulations of the natural- and deep-breathing states. In the former, the roles and functions of the nasal structural elements were deduced in association with the airflow characteristics in each element, and in the latter, a computational modeling method was presented for evaluating nasal patency experimentally by rhinomanometry. Through the natural- and deep-breathing computations, the roles and functions of the nasal elements were again evaluated with correlation to the nasal resistance; the aim was to establish an objective method for evaluating nasal obstruction.

MATERIALS AND METHODS

Rhinomanometry

To measure nasal patency experimentally, we used the nozzle anterior method in rhinomanometry. In deep respiration, the volume flow rate at one nostril of the target nasal cavity was measured by a flow sensor, while the other nostril was filled with a cock containing a pressure sensor, which is considered as measuring the pressure in the choana because the right and left nasal cavity unite in the vicinity of the choana. When the pressure difference ΔP is 100 Pa, the resistance for the target nasal cavity is defined as

$$R = \Delta P/V, G = 1/R, \quad (1)$$

where R [Pa·s/cm³] is the nasal resistance, ΔP is the

pressure difference between the atmosphere and the choana, V [cm³/s] is the volume flow rate, and G [cm³/(Pa·s)] is the conductance.

Having obtained the resistance for each cavity, the right resistance R_{right} and the left resistance R_{left} were calculated, and the total resistance R_{total} for both cavities was calculated as

$$1/R_{\text{total}} = 1/R_{\text{right}} + 1/R_{\text{left}}. \quad (2)$$

Procedure and Modeling Methods

We began by creating a computer-generated intranasal model using nasal-cavity computed tomography (CT) scans (performed with a section width of 0.3 mm) of a 32-year-old male who had undergone septoplasty. Nasal septal deviation is individually different in the size and location. In this document, we study the inferior turbinate, middle turbinate and superior turbinate that have comparatively small individual difference. So we use the model after the septoplasty that are not affected from nasal septal deviation. We subsequently used CFD to simulate the airflow numerically in the natural- and deep-breathing states, and we quantified the nasal-cavity patency based on the numerical results. We also performed experimental rhinomanometry for ground-truth measurement on the adult male whose CT images had been obtained, and we compared these results with those of numerical simulations.

CFD is a technique used to quantify airflow (in addition to other parameters) computationally using the Navier–Stokes equations, which are the governing equations of viscous fluid motion. The CFD workflow was as follows.

1) Generation of geometric model

We used the general-purpose drawing software AutoCAD (Autodesk, Inc., USA) to create a three-dimensional model of the nasal cavity of an adult male based on nasal-cavity CT scans performed with a section width of 0.3 mm (Fig. 1).

2) Grid generation

In CFD, the object shapes and surrounding space must be discretized and represented by grids, for

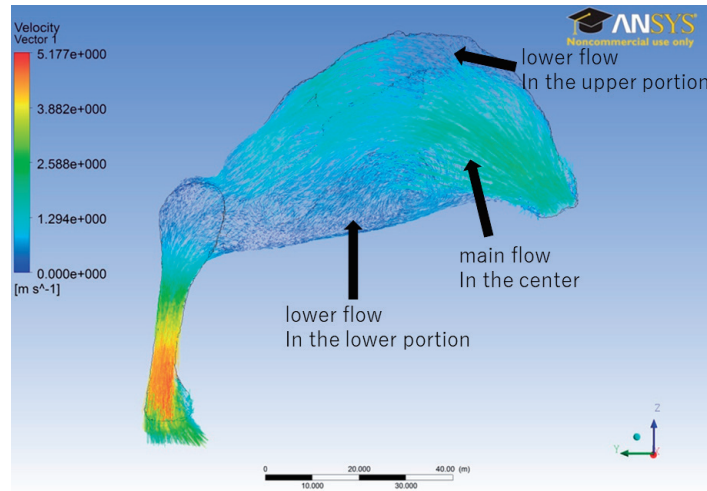


Fig. 2 Inhalation streamlines in the left nasal cavity
The main flow was in the center. There was lower air flow in the upper and lower portion.

which we used the ANSYS ICEM CFD software (ANSYS, Inc., USA). The vicinity of the nasal surface is covered with five layers of prism elements, while the interior region is covered with tetra elements. The total number of cells was set at 4,195,233 after confirming grid convergence in the flow calculations.

3) Flow analysis

We used the Navier–Stokes equations and the continuity equation as the governing equations for analyzing incompressible viscous flow within the nasal model, and we used ANSYS FLUENT to perform the numerical simulations. The finite-volume method was adopted with discretization of a Semi-Implicit Method for Pressure-Linked Equations method.

In the natural-breathing computation, we considered only steady-state flow because, according to Ref. [10], numerical results for unsteady and steady maximum respiration exhibited no notable discrepancy because the Womersley number was relatively low. We imposed the following boundary conditions:

- i) the pressure at the nostrils was zero (i.e., atmospheric pressure);
- ii) on the trachea side, the velocity was 1.13 m/s at maximum inhalation and exhalation, which was computed from the maximum velocity of 2.3 m/s at the nostril during quiet respiration;
- iii) the velocity was zero at the nasal wall.

To model the rhinomanometry measurements in the deep-breathing computation, we considered unsteady flow with the following boundary conditions:

- i) the pressure at the nostril of the target nasal cavity was zero (i.e., atmospheric pressure), while the other nostril was closed and treated as a wall;
- ii) on the trachea side, the unsteady velocity was given by $v_{\max} \cos(2\pi t/T)$ to evaluate the nasal patency, where the maximum velocity was $v_{\max} = 8$ m/s, the period was $T = 3$ s, and t [s] was time;
- iii) the velocity was zero at the nasal wall.

4) Visualization

Visualization is a technique used to capture invisible flows as a visual image. Of the various visualization methods that exist, we used numerical–analytical sim-

ulation.

5) Patency evaluation

Ground-truth measurements were performed using rhinomanometry by the nozzle anterior method. To model the rhinomanometry measurements, we quantified the nasal-cavity patency using Eqs. (1) and (2) in the deep-breathing computation, and we compared the results with those measured experimentally.

RESULTS

Natural breathing (steady solution)

The CFD results for the inhalation airflow in the left nasal cavity are shown in Fig. 2. The airflow was higher in the center of the nasal cavity and lower in the upper and lower portions. We also performed multiple sagittal sections to evaluate/review the airflow within the entire nasal cavity. Figure 3a shows the cross section of the common nasal meatus near the nasal septum, demonstrating that the airflow was higher in the center of the nasal cavity and lower at the choana (Fig. 3a). Furthermore, as observed in the same cross section, the airflow in front of the olfactory cleft formed a loose vortex (Fig. 3a, ○). A cross section taken slightly on the lateral side of the common nasal meatus (Fig. 3b) showed that the center of the airflow corresponded to the center of the nasal cavity, and a loose vortex (Fig. 3b, ○) formed in the lower portion of the nasal cavity near the front of the inferior turbinate. In a cross section (Fig. 3c) in which the middle/inferior meatus was visible, most of the airflow passed through the middle meatus, and a small vortex forms in front of the inferior turbinate (Fig. 3c, ○).

The CFD results for the exhalation airflow in the left nasal cavity are shown in Fig. 4. We evaluated the exhalation airflow within the nasal cavities by taking multiple sagittal sections as we did in the case of inhalation. In the cross section of the common nasal meatus near the nasal septum (Fig. 5a), most of the airflow passed through the upper portion of the nasal cavity, and a vortex forms in front of the olfactory cleft (Fig. 5a, ○). Although this was also observed during inhalation, it differed here in that the direction of the vortex was then counterclockwise. Furthermore,

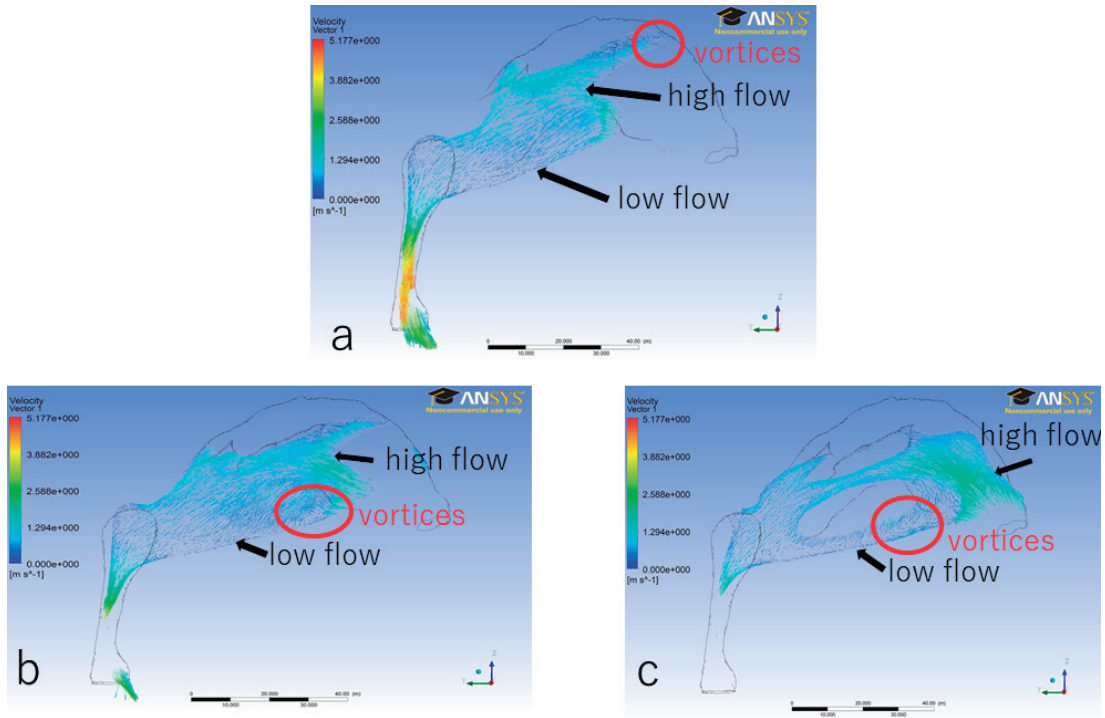


Fig. 3 Sagittal sections with nasal velocity vectors during inhalation (a) The cross-section of the common nasal meatus near the nasal septum. A loose vortex was observed in the olfactory cleft(○). (b) The cross-section on a slightly lateral side of the common nasal meatus. Loose vortices were observed in the lower portion of the nasal cavity and near the front of the inferior turbinate (○). (c) Cross-section through the middle/inferior meatus. Loose vortices was observed in front of the inferior turbinate (○).

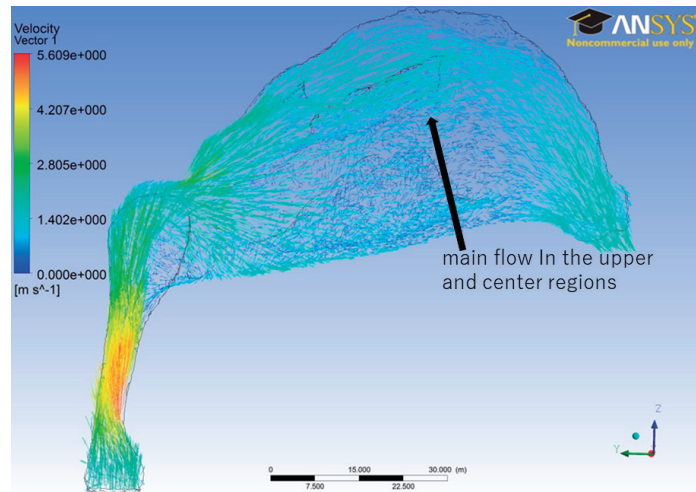


Fig. 4 Exhalation streamlines in the left nasal cavity
The main flow was in the upper and center regions.

the flow tended to be slower compared to that in other areas in the upper portion of the nasal cavity. A cross section taken slightly on the lateral side of the common nasal meatus (Fig. 5b) showed that most of the airflow passed through the upper nasal cavity, and multiple vortices form at the back of the nasal cavity (Fig. 5b, ○). Cross sections of the middle/inferior meatus (Fig. 5c) showed that the most of the airflow passed through the upper nasal cavity, with the flow speed in the middle/inferior meatus being relatively low.

Deep breathing (unsteady solution for evaluating nasal patency)

The CFD results for the nasal patency are presented

in Figs. 6 and 7 and Tables 1 and 2. Comparing both sides, we found the right side to be more patent than the left, with the experimental measurements exhibiting the same tendency. However, the CFD and experimental measurements differed when the nasal-cavity pressure was approximately -100 Pa in inhalation. The CFD and experimental measurements gave the resistance for the right nasal cavity to be 0.191 and 0.26, respectively, that for the left nasal cavity to be 0.24 and 0.33, respectively, and that for both nasal cavities to be 0.104 and 0.15, respectively.

In addition, we evaluated the pressure in the nasal cavity when evaluating the nasal resistance during inhalation. The parameter values used to measure the

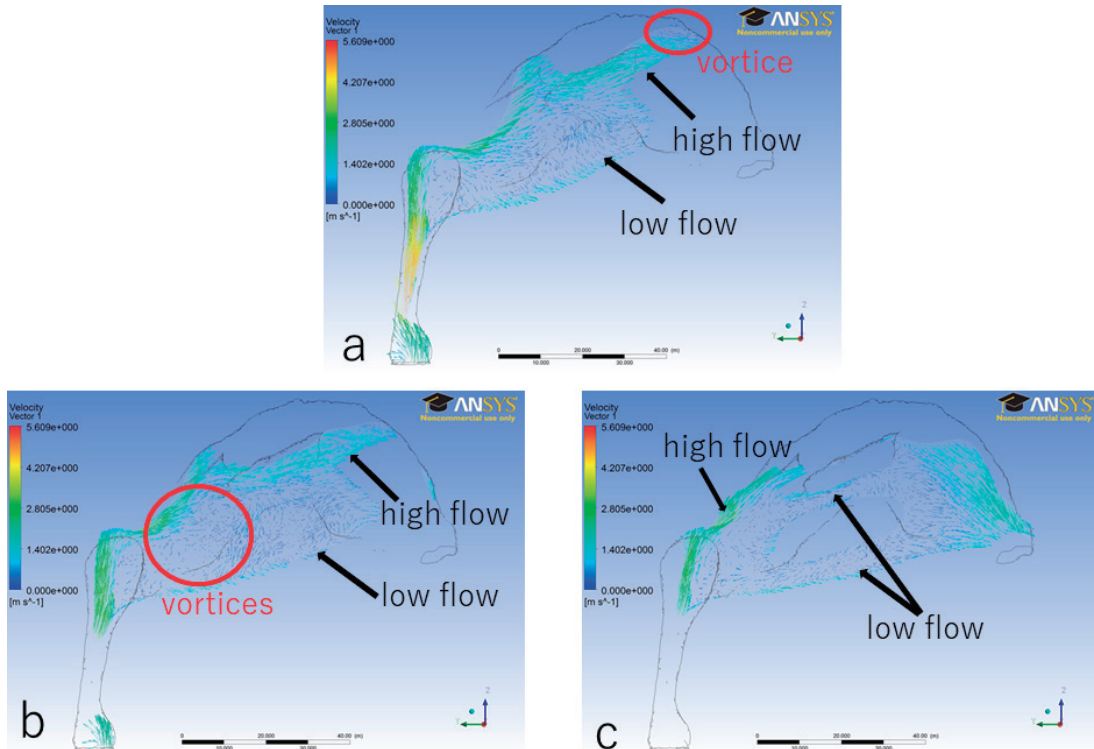


Fig. 5 Sagittal sections with nasal velocity vectors during exhalation (a) The cross-section of the common nasal meatus near the nasal septum. The formation of a vortex was observed in front of the olfactory cleft (○). (b) The cross-section on a slightly lateral side of the common nasal meatus. The formation of multiple vortices was observed at the back of the nasal cavity (○). (c) Cross-sections of the middle/inferior meatus.

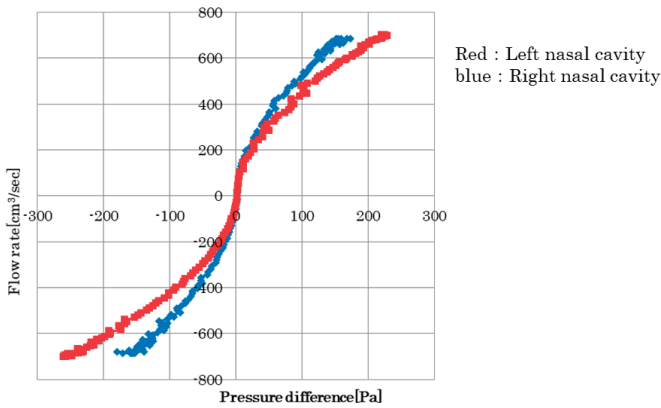


Fig. 6 Nasal resistance of the right and left nasal cavities measured using CFD.

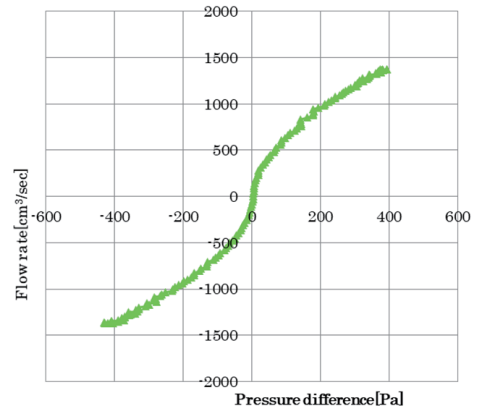


Fig. 7 Nasal resistance in both nasal cavities measured using CFD.

nasal resistance are given in Table 1 for a choana pressure of approximately -100 Pa. The right and left nasal resistances were normal. The pressures in the left and right nasal cavities were shown in Figs. 8 and 9, respectively; these were the pressure distributions at a choana pressure of approximately -100 Pa. The pressure was zero at the nostril and highest in the nasal cavity. In the coronal sections of the left nasal cavity, the roof of the nasal cavity and the olfactory cleft were where the pressure was highest, followed by the middle meatus and in front of the middle meatus (Fig. 8a, ○). The pressures in the lower common meatus and inferior meatus were relatively low (Fig. 8a, →). At the surface wall, the olfactory cleft was where the pressure was highest, followed by the roof of the nasal cavity and the middle meatus (Fig. 8b, c, ○). In the coronal sec-

tions of the right nasal cavity, the front of the middle meatus was where the pressure was highest, followed by the olfactory cleft (Fig. 9a, ○). At the surface wall, the front of the middle meatus, the olfactory cleft, and the middle meatus were where the pressure was highest (Fig. 9b, c, ○). In both nasal cavities, the nasal valve was a region of relatively low pressure (Fig. 8b, △, 9b, △), having the same pressure as the inferior meatus.

DISCUSSION

CFD had been applied in several fields, with various studies in rhinology having reported its use [15]. CFD could be a useful tool for visualizing pressure, velocity, and other invisible parameters, making it suitable for evaluating nasal physiology. Eiting *et al.* [16] used computer-based simulation to compare the veloc-

Table 1 CFD parameters in the right and left nasal cavity shown in Fig. 8.

		Flow rate [cm ³ /s] 10°C	Pressure [Pa]	Resistance [Pa/cm ³ /sec]	Conductance [cm ³ /s/Pa]
Left	Inspiration	-520.2	-148.1	0.2847	3.512
		-423.4	-101.8	0.2405	4.158
		-468.4	-104.5	0.2230	4.484
	-298.0	-49.73	0.1669	5.993	
	Expiration	566.3	151.9	0.2682	3.729
		479.2	99.26	0.2071	4.828
310.7		47.49	0.1529	6.541	
		Flow rate [cm ³ /s] 10°C	Pressure [Pa]	Resistance [Pa/cm ³ /sec]	Conductance [cm ³ /s/Pa]
Right	Inspiration	-671.2	-150.9	0.2248	4.449
		-537.7	-103.1	0.1918	5.214
		-555.1	-110.6	0.1990	5.025
	-379.8	-50.48	0.1330	7.523	
	Expiration	664.5	149.2	0.2246	4.453
		519.4	99.67	0.1919	5.211
355.4		50.50	0.1421	7.038	

Table 2 CFD parameters in both nasal cavities shown in Fig. 9.

		Flow rate [cm ³ /s] 10°C	Pressure [Pa]	Resistance [Pa/cm ³ /sec]	Conductance [cm ³ /s/Pa]
Both	Inspiration	-1191	-150	0.1259	7.943
		-961.1	-100	0.1040	9.611
		-677.8	-50	0.07377	13.56
	Expiration	1230	150	0.1219	8.206
		998.6	100	0.1001	-9.986
		666.1	50	0.07506	13.32

ities in the reduced olfactory recess, normal olfactory recess, and enlarged olfactory recess of a bat (*Carollia perspicillata*), concluding that an enlarged olfactory recess led to low air flow and velocity and that this could play an important role in improving the residence time of odorants within the olfactory region. Lawson *et al.* [17] reported that a long residence time improved absorption efficiency, implying that proportionally more odorant molecules were absorbed in the mucus. Wei *et al.* [18] used CFD to compare the nasal cavity of a normal Sprague Dawley rat with one subjected to artificial widening; the average air velocity in the normal cavity was higher than that in the artificially widened one. In the present study, we observed decreased airflow speed

and the formation of a vortex in front of the olfactory cleft, which was where the pressure was highest, and therefore, lowest pressure difference with the nostril, and low resistance.

This was based on the following perspective: from the definition of nasal resistance, the pressure distribution at inhalation could be converted, by taking the difference between local pressure and the atmospheric pressure at the nostril, into resistance distribution from the nostril to the choana, at which the value showed that of the nasal resistance. No study has yet reported that pressure and resistance might be related to olfaction. Therefore, our results may be relevant to understanding the connection between olfaction and

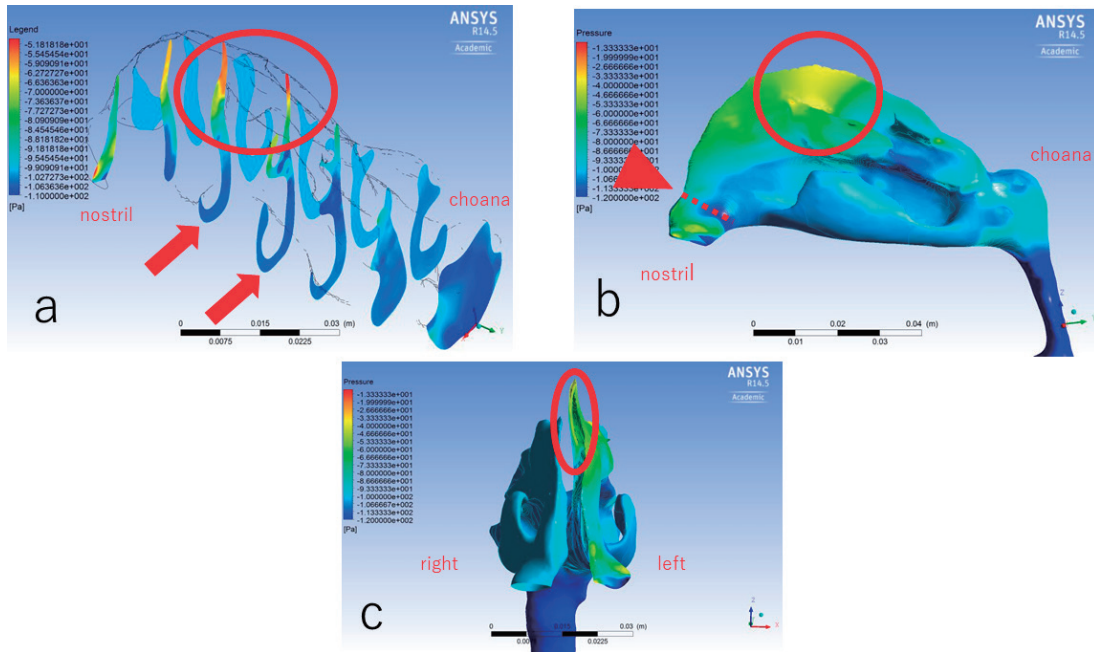


Fig. 8 Pressure in the left nasal cavity (a) Multiple coronal sections of pressure in the left nasal cavity. The highest pressure was in front of the middle turbinate and the second highest pressure was at the olfactory cleft (a ○). (b) Pressure at the surface of the wall from a lateral view. (c) Pressure at the surface of the wall from a frontal view. High pressure was found in the middle meatus and olfactory cleft (b, c ○). Nasal valve pressure was low (b △).

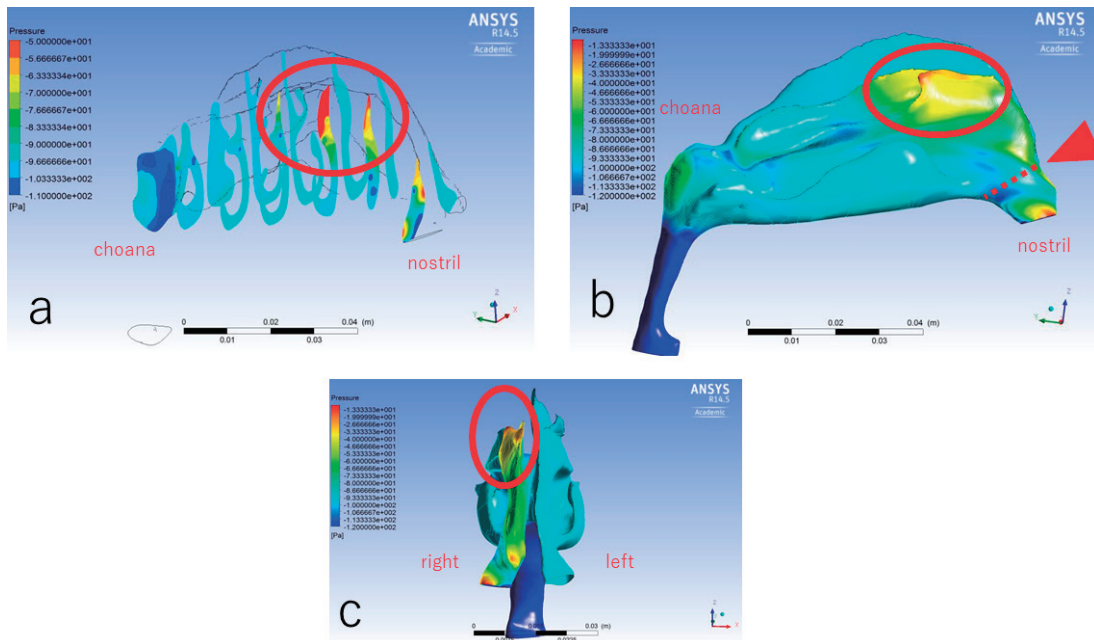


Fig. 9 Pressure in the right nasal cavity (a) Multiple coronal sections of pressure in the right nasal cavity. The front of the middle meatus had the highest pressure and the olfactory cleft had the second highest (○). (b) Pressure at the surface of the wall from a lateral view. (c) Pressure at the surface of the wall from a frontal view. The front of middle meatus, the olfactory cleft, and the middle meatus had the highest pressure (b, c ○). Nasal valve pressure was low (b△).

other functions via velocity, pressure, and resistance.

The middle meatus exhibited the most ostia among the paranasal sinuses. In comparison to the inferior meatus, the middle meatus exhibited a higher flow speed during inhalation and the formation of multiple small vortices during exhalation. In addition, the pressure there at inhalation was relatively high, and the resistance was relatively low, thereby suggesting its

association with paranasal sinus ventilation. Thieme *et al.* reported the feasibility of using dual energy CT and dynamic CT for imaging the ventilation of the paranasal sinuses in a nasal cast using xenon gas [19], and previous studies have used that method to evaluate paranasal ventilation [20–23].

The function of the nasal valve is to create a vortex at the olfactory cleft and suppress counterflow at the

inferior meatus [10]. We found low pressure at the nasal valve and the inferior meatus, and therefore a high pressure difference there, along with high resistance. This is consistent with the function of the nasal valve.

Using numerical simulations, Hariri *et al.* showed that reducing the inferior turbinate volume improved the nasal resistance [24]. We found low pressure and high resistance around the inferior turbinate, thereby supporting the observation by Hariri *et al.* The nasal valve and the inferior turbinate might, thus, play an important role in nasal resistance.

We observed the formation of a vortex around the nasal valve, which because it slowed that the flow was thought to cause airflow retention; i.e., the airflow would remain for a relatively long time in this area. This suggested that the vortex was associated with humidification, warming of the nose, and dust elimination. Using CFD, Zhao *et al.* showed that the gradient of heat loss was not uniform but was concentrated in the nasal valve and vestibule region [25]. The vortex might be responsible for differing heat loss in this region, to which the direction of the vortex against the nasal-cavity wall might be related.

At present, rhinomanometry and acoustic rhinometry are used to measure nasal patency for evaluating nasal obstruction. Here using the presented computational method for modeling rhinomanometry measurements, we conducted an unsteady numerical simulation and evaluated the nasal-cavity resistance quantitatively. From the results, the resistance measured experimentally was larger by approximately 50% than that obtained using CFD. We hypothesized that the main reason for this was that the flow meter inserted into the target nostril makes the nostril effectively smaller, thereby increasing the resistance. However, the qualitative tendency was similar between computation and experiment in that the right nasal cavity was more patent than the left one. The results obtained from using CFD methods suggested a way to objectively evaluate the airflow dynamics in the nasal cavity from the perspective of respiratory physiology and anatomy.

We reason that the evaluation method described herein not only combines the advantages of rhinomanometry and acoustic rhinometry but also compensates for their disadvantages. In addition, it may be possible using this method. Moreover, this method may be used for preoperative simulation to assess the most effective surgical approach as well as for post-operative evaluation. However, future studies will need to involve far more cases of nasal patency simulation before the CFD method can be used to evaluate objectively the subjective symptoms of patients with nasal obstruction and nasal airflow problems, as well as for pre-/post-operative simulation during surgical treatment.

CFD method is very complicated for otolaryngologist. 3D model creation and CFD need special software. So for the spread of this method, it need to change for easy and specialized method for otolaryngologist.

CONCLUSION

To seek an objective method for evaluating nasal obstruction, we presented a computational method for modeling the experimental results of rhinomanometry to evaluate nasal patency, and we conducted numerical simulations of the natural- and deep-breathing states.

Regarding the nasal patency, the qualitative tendency was similar between computation and experiments, but the quantitative accordance was unsatisfactory. Through natural- and deep-breathing computations, the roles and functions of the olfactory region, nasal valve, and middle and inferior meatuses were evaluated by using flow patterns and pressure with correlation to the nasal resistance and physiology. Above all, in deep-breathing computation using the present computational modeling, it was deduced that the pressure difference is essential for determining the nasal sites at which the nasal resistance is produced. Thus, numerical simulation with the present computational modeling could be an objective method for evaluating nasal obstruction. However, further studies are needed in which nasal airflow is evaluated with more patients.

ACKNOWLEDGEMENTS

The authors would like to thank Enago (www.enago.jp) for the English language review.

REFERENCES

- 1) Merkle J, Kohlhas L, Zadoyan G, Mösger R, Hellmich M. Rhinomanometric reference intervals for normal total nasal airflow resistance. *Rhinology* 2014; 52(4): 292-299.
- 2) Sakata T, Tanaka G, Sera T, Kakusho N, Yokota H, Ono K, *et al.* Voxel simulation of nasal cavity, The Proceedings of 22nd Bioengineering Conference, The Japan Society of Mechanical Engineers, 2010.
- 3) Horschler I, Meike M, Schroder W. Numerical Simulation of the flow field in a model of the nasal cavity. *Computer and Fluids* 2003; 32: 39-45.
- 4) Keyhani K, Scherer PW, Mozell MM. Numerical Simulation of airflow in the human nasal cavity. *J Biomech Eng* 1995; 117(4): 429-441.
- 5) Wakayama T, Suzuki M, Tanuma T. Effect of Nasal Obstruction on Continuous Positive Airway Pressure Treatment: Computational Fluid Dynamics Analyses. *PLoS One* 2016; 11(3); doi: 10.1371/journal.pone.0150951.
- 6) Izumi Y, Tajikawa T, Ohba K, Uesugi Y. In vitro experiment on reciprocating flow in a model of the nasal cavities and pharynx. The Proceedings of the 19th Bioengineering Conference, The Japan Society of Mechanical Engineers 2007.
- 7) Rennie C.E., Hood C.M., Blenke E.J.S.M., Schroter R.S., Doorly, D.J., Jones H, *et al.* Physical and computational modeling of ventilation of the maxillary sinus. *head and neck surgery* 2011; 145(1): 164-170.
- 8) Afiza E, Kurashina Y, Takakura Y, Atsumi T, Iida M. Investigation of airflow patterns within real and simplified models of nasal cavities, The 12th International Symposium on Fluid Control, Measurement and Visualization. *FLUCOME* 2013.
- 9) Afiza A, Takakura Y, Atsumi T, Iida M. Airflow patterns within real and 3D simplified models of nasal cavities (I. Experimental Study). *Proc Schl Tokai Univ* 2015; 40: 97-108.
- 10) Afiza A, Takakura Y, Atsumi T, Iida M. Airflow patterns within real and 3D simplified models of nasal cavities (II. Numerical Study). *Proc Schl Tokai Univ* 2015; 40: 109-119.
- 11) Afiza A, Takakura Y, Atsumi T, Iida M. A Study on ostia variation for airflow patterns within nasal cavity models with maxillary sinus. *Proc Schl Tokai Univ* 2015; 40: 89-96.
- 12) Afiza A, Takakura Y, Iida M. Function of ostia in airflow patterns within nasal cavity model with maxillary sinus. *ASRJETS* 2016; 21(1): 41-60.
- 13) Kaneda S, Iida M, Yamamoto H, Sekine M, Takakura Y. Evaluation of nasal airflow and resistance: a study of experimental and computational modelling. *Rhinology World Congress, ISIAN and IRS* 2017.
- 14) Takada S, Takakura Y, Atsumi T, Iida M. Unsteady numerical simulation of respiratory flows within a nasal-cavity model. *Proceedings of the 26th bioengineering conference, Annual Meeting of BED, JSME* 2014; 525-526.

- 15) Kim SK, Na Y, Kim JI, Chung SK. Patient specific CFD models of nasal airflow: Overview of methods and challenges. *J Biomech* 2013; 46(2): 299-306.
- 16) Eiting TP, Smith TD, Perot JB, Dumont ER. The role of the olfactory recess in olfactory airflow. *J Exp Biol* 2014; 217(10): 1799-1803.
- 17) Lawson MJ, Craven BA, Paterson EG, Settles GS. A computational study of odorant transport and deposition in the canine nasal cavity: implications for olfaction. *Chem Senses* 2012; 37(6): 553-566.
- 18) Wei Z, Xu Z, Li B, Xu F. Numerical simulation of airway dimension effects on airflow patterns and odorant deposition patterns in the rat nasal cavity. *PLoS One* 2013; 8(10): e77570. doi: 10.1371/journal.pone.0077570.
- 19) Thieme SF, Möller W, Becker S, Schuschnig U, Eickelberg O, Helck AD, *et al.* Ventilation imaging of the paranasal sinuses using xenon-enhanced dynamic single-energy CT and dual-energy CT: a feasibility study in a nasal cast. *Eur Radiol*, 2012; 22(10): 2110-2116.
- 20) Moeller W, Schuschnig U, Meyer G, Häussinger K, Keller M, Junge-Hülsing B, *et al.* Ventilation and aerosolized drug delivery to the paranasal sinuses using pulsating airflow- a preliminary study. *Rhinology* 2009; 47(4): 405-412.
- 21) Möller W, Lübbers C, Münzing W, Canis M. Pulsating airflow and drug delivery to paranasal sinuses. *Curr Opin Otolaryngol Head Neck Surg* 2011; 19(1): 48-53.
- 22) Möller W, Schuschnig U, Khadem Saba G, Meyer G, Junge-Hülsing B, Keller M, *et al.* Pulsating aerosols for drug delivery to the sinuses in healthy volunteers. *Otolaryngol Head Neck Surg* 2010; 142(3): 382-388.
- 23) Möller W, Schuschnig U, Meyer G, Mentzel H, Keller M. Ventilation and drug delivery to the paranasal sinuses: studies in a nasal cast using pulsating airflow. *Rhinology* 2008; 46(3): 213-220.
- 24) Hariri BM, Rhee JS, Garcia GJ. Identifying patients who may benefit from inferior turbinate reduction using computer simulations. *Laryngoscope* 2015; 125(12): 2635-2641.
- 25) Zhao K, Blacker K, Luo Y, Bryant B, Jiang J. Perceiving nasal patency through mucosal cooling rather than air temperature or nasal resistance. *PLoS One* 2011; 6(10): e24618. doi: 10.1371/journal.pone.0024618.